Modeling of cracking during pultrusion of large-size profiles

Alexander Safonov[1*], Mikhail Gusev[1], Anton Saratov[2], Alexander Konstantinov[3],

Ivan Sergeichev[1], Stepan Konev[1], Sergey Gusev[1], Iskander Akhatov[1]

[1]Center for Design, Manufacturing and Materials, Skolkovo Institute of Science and Technology, Moscow, Russia

[2]DATADVANCE, Moscow, Russia

[3]Research Institute of Mechanics, Nizhny Novgorod State University, Nizhny Novgorod, Russia

Corresponding Author: Alexander A. Safonov, PhD

*Corresponding Author E-mail: a.safonov@skoltech.ru

Keywords: pultrusion, epoxy, process optimization, cracking, numerical simulation

Abstract

The pultrusion of large-diameter glass fiber reinforced epoxy rods at high pulling speed is often accompanied by the formation of cracks at the surface of a profile, leading to product rejection. In this study, we investigate the causes of crack formation based on numerical simulations of manufacturing process mechanics, including the temperature distribution, degree of polymerization, and residual stresses. Based on the built model, we solve the problem of temperature condition optimization for maximizing pulling speed. The results show that up to 27% increases in pulling speed are possible provided that the following conditions are met: thermal destruction of the material is avoided; a profile is cooled sufficiently quickly before cut-off; a high degree of polymerization is achieved in a final product; and there are no cracks in a profile.

Introduction

Pultrusion is a high-production process allowing the fabrication of high-performance composite profiles having a constant cross section. Profiles that are produced possess low defect levels and virtually invariable quality across a whole production batch fabricated over several days, with the total length of the profile amounting to several kilometers [1,2]. In the thermoset pultrusion process, pre-impregnated reinforcing material is constantly pulled through a heated die block, where the profile is formed, heated, and polymerized. Continuous pulling is provided by a pulling unit. As the process is automated and virtually independent of human factor influences, the quality of the product will be predominantly determined by the correct selection of manufacturing parameters at the start of the process. To maximize the efficiency of the process, we have to maximize the pulling speed; however, an increase in pulling speed may result in defects such as incomplete polymerization, cracking, and damage to the profile by pulling grips or by the cut-off unit owing to the high temperature of the profile [3]. Therefore, incorrectly set process parameters (such as pulling speed and the temperatures at the forming die) may result in the whole batch being rejected.

In engineering practice, optimum parameters are found by trial-and-error based on the expertise of engineers and the knowledge of basic rules-of-thumb outlined in manuals [4,5]. In academia, there is currently a steadily growing trend toward the development of methods of numerical simulation for processes taking place during pultrusion [6,7]. These include thermal conductivity and matrix polymerization [8], the impregnation of reinforcing material with resins during injection [9–11], pressure distribution within a forming die [12], the pulling force [13], and residual stress-strain state in a pultruded profile [14,15]. Based on these models, new methods of realizing manufacturing process optimization are developed in order to maximize the process output and to reduce the power consumption [16,17].

Of special interest is the pultrusion of profiles with large cross-section area to perimeter ratios. As polymer matrix composites have low thermal conductivity, there is a specific time lag between the curing of the matrix at the surface of the profile and within the bulk of the profile. Such processes usually feature low productivity. Therefore, achieving pulling speed maximization is a priority in the mass production of such profiles. However, if the pulling speed is too high, the profile exiting the die block will have only a thin layer of cured material at its surface, while the bulk of the polymer will remain in liquid form [18–20]. The pressure resulting from the thermal expansion of the liquid matrix will be sufficient to break the thin crust of the polymerized material, resulting in a long lengthwise crack with the liquid matrix escaping through the crack. Figure 1 shows the crack on the surface of an 80 mm diameter glass-fiber reinforced rod after the die block exit. A very high temperature at the die block or a high accelerator content may result in the release of large amounts of heat during the exothermic reaction, leading to thermal destruction of the material [21,22]. In addition, if temperature conditions at the die block are set so that the profile is fully cured within the die block, the significant temperature difference between the composite material and the die block may result in a significant increase in the required pulling force. Therefore, optimum conditions are set so that the exothermic peak occurs at a certain distance after the die exit. Further, to prevent mechanical damage of the profile, the pulling speed should be selected so that the profile is cooled below the glass transition temperature before the cutting stage.

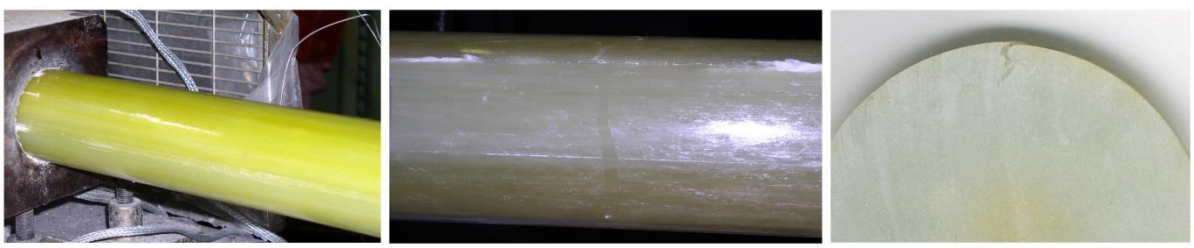

(a) (b) (c)

Figure 1. Formation of crack during pultrusion of 80 mm diameter GFRP rod: (a) – initiation of crack after the die block exit; (b) – opening of the crack as the profile is pulled further; (c) – cross-section of the cracked pultruded rod.

Considering the large number of processing parameters, including the pulling speed, temperature distribution at heating zones, temperature at the die entrance, combination of reinforcement types, and resin composition, it becomes important to develop a mathematical model that describes the large-size profile pultrusion in order to optimize the processing parameters. On the one hand, such a model should describe non-uniformities in the distribution of polymer phases (liquid, rubber-like, glassy) and distributions of the temperature, curing degree, and residual stress fields. It is desirable to implement the model within a single computational space, allowing routine engineering calculations and the multi-criteria optimization to be conducted for arbitrary profile types. This research is original in that it attempts to develop a mathematical model and its numerical implementation together with the optimization module, based on predictions of the finished part quality.

The proposed model of the pultrusion process is based largely on previously developed and tested approaches to the modeling of thermal conductivity, curing degree, and residual stresses, as described in the review article together with corresponding references [7]. Listed below are some of the improvements to pultrusion simulation methods that are proposed in this article.

1. Available publications that describe constitutive equations for the mechanical behavior of a composite in pultrusion during variations in temperature and degree of polymerization assume that the Poisson coefficient remains constant [14]. However, there is a series of publications which clarify that the Poisson's ratio of a matrix tends to 0.5 during transition to the rubber-like state [23,24]. Besides, although the Young's modulus decreases by several orders of magnitude during transition to the rubber-like state, the bulk compression modulus demonstrates a decrease of only 2.5 times [23,25].

2. The majority of available publications on pultrusion simulations did not analyze residual stress distributions in their reports of process-induced defects such as cracks, as previous research efforts focused primarily on the prediction of profile warpage [15] and on the calculation of residual stress levels to account for their influence on the strength of structures under service loads [26]. However, there are several publications that simulate cooling-induced fracture in vacuum-infused parts after curing [27], where residual stresses after cooling are substituted into strength criteria together with material properties under normal conditions. In this work, we study the formation of cracks immediately after matrix polymerization. To do this, we use the relationship between the strength of the composite material and the temperature, while verifying the strength criterion compliance during the whole simulation process.

3. Earlier publications presented results of process parameter optimization based on polymerization and heat conductivity simulations [17,28–30], where the final degree of polymerization and maximum temperature were considered as quality criteria. Here, in addition to the final degree of polymerization and maximum temperature, we also consider supplemental quality criteria that account for cracking and the overheating of materials at the end of the pulling process.

Thus, the novelty of this work lies in the description of crack formations during the pultrusion of large-size profiles based on mechanical simulations of composite formation during pultrusion pulling. In addition, the optimization of process parameters is presented based on the mathematical model that was developed.

Methods

During the simulations, we computed the degree of curing and temperature distributions, which were then used to compute the stress-strain state in a composite [14]. To accelerate the computations, we considered a two-dimensional (2D) setting both for the problems of thermal conductivity and the degree of polymerization distribution [31], as well as for the problem of stress-strain state calculations [32]. All of the calculations presented here are conducted for a transversely isotropic composite material. The anisotropic axis of the material coincides with the pulling direction and with the orientation of unidirectional rovings. The axis of anisotropy coincides with the OZ axis of the Cartesian coordinate system, with the OX- and OY-axes lying in the cross-sectional plane of the profile.

2D Thermal Model

Here, we consider a stationary pulling process with a pulling speed u. The heat conductivity equation for the profile during pultrusion, in the Lagrangian (material) frame of reference, can be expressed as follows, disregarding the longitudinal conduction [31]:

$$\rho_c C_{pc}(T,\alpha)\frac{\partial T}{\partial t} = k\frac{\partial^2 T}{\partial x^2} + k\frac{\partial^2 T}{\partial y^2} + q, \quad (1)$$

where x and y are the cross-sectional coordinates; T represents the temperature; $C_{pc}(T,\alpha)$ is the specific heat of composite material depending on the degree of polymerization and temperature; ρ_c is the density of a composite material; and k is the thermal conductivity of a composite material in the cross-sectional plane. It should be noted that as the process equation is expressed in the Lagrangian frame of reference, the linear speed, u, is absent from (1) and appears in boundary conditions [31]. Boundary conditions determine the interactions between the moving profile and the die block and the ambient air. The convective boundary conditions were used in computations:

inside the die: $k\frac{\partial T}{\partial n}\Big|_{\Gamma} = -h_{die}\big(T - T_{die}(z)\big)$; (2)

outside the die: $k\frac{\partial T}{\partial n}\Big|_{\Gamma} = -h_{air}(T - T_{amb})$; (3)

where Γ is the surface of the profile, $h_{die}$is the coefficient of convective heat transfer between the die block and the profile, h_{air} is the coefficient of convective heat transfer between the ambient air and the profile after exiting the die block, T_{die} is the temperature of the metallic die block, which varies along the direction of pulling, z, and T_{amb} is the ambient temperature. The temperature of the material at the die entrance, T_{in}, is set assuming its uniformity in a cross section:

$$T|_{t=0} = T_{in} \quad (4)$$

The temperature of the material at the die entrance, T_{in}, is set assuming its uniformity in a cross section:

$$q = \rho_r\big(1 - V_f\big)H_R\frac{d\alpha}{dt}, \quad (5)$$

where ρ_r is the density of resin, H_R is the total heat released during curing, V_f is the volume fraction of reinforcement in a composite, $\frac{d\alpha}{dt}$ is the curing rate of the resin, and α is the degree of curing. The degree of curing is determined by the ratio of current heat released, $\mathrm{H(t)}$, to the total heat released during curing, $\mathrm{H_R}$, i.e., $\alpha = \mathrm{H(t)/H_R}$. The curing degree rate can be expressed using the Arrhenius type equation as follows:

$$\frac{d\alpha}{dt} = A_0\exp\left(-\frac{E_a}{RT}\right)(1-\alpha)^n, \quad (6)$$

where $\mathrm{A_0}$ is the pre-exponential coefficient; $\mathrm{E_a}$ is the activation energy; n is the order of the reaction; and R is the universal gas constant.

We assume that preheating the material before the die entrance will not result in significant polymerization of the resin; hence, the degree of material polymerization at the die entrance, T_{in}, is taken to be zero:

$$\alpha|_{t=0} = 0. \quad (7)$$

2D Mechanical Model

To describe the mechanical behavior of the matrix during curing, we use the Cure Hardening Instantaneous Linear Elastic (CHILE) model [33], which accounts for changes in the elastic modulus during phase transitions. The following form of the relationship for the resin elastic modulus is used:

$$E_m(T^*) = \begin{cases} E_m^0, & T^* > \mathrm{T_{g\infty}} - 20\ ℃; \\ E_m^1 + \frac{T^* - (\mathrm{T_{g\infty}} - 40\ ℃)}{20℃}(E_m^0 - E_m^1), & \mathrm{T_{g\infty}} - 20\ ℃ \geq T^* > \mathrm{T_{g\infty}} - 40\ ℃; \\ E_m^2 + \frac{T^* - (\mathrm{T_{g\infty}} - 60\ ℃)}{20℃}(E_m^1 - E_m^2), & \mathrm{T_{g\infty}} - 40\ ℃ \geq T^* > \mathrm{T_{g\infty}} - 60\ ℃; \\ E_m^3 + \frac{T^* - (\mathrm{T_{g\infty}} - 80\ ℃)}{20℃}(E_m^2 - E_m^3), & \mathrm{T_{g\infty}} - 60\ ℃ \geq T^* > \mathrm{T_{g\infty}} - 80\ ℃; \\ E_m^\infty + \frac{T^*}{\mathrm{T_{g\infty}} - 80\ ℃}(E_m^3 - E_m^\infty), & \mathrm{T_{g\infty}} - 80\ ℃ \geq T^* > 0\ ℃; \\ E_m^\infty, & T^* \leq 0\ ℃ \end{cases} \quad (8)$$

where $T^* = T_g(\alpha) - T$; E_m^0, E_m^1, E_m^2, E_m^3, and E_m^∞ represents the elastic modulus of polymerized matrix at temperatures of 20 ℃, 40 ℃, 60 ℃, 80 ℃, and $\mathrm{T_{g\infty}}$, respectively. Further, term $T_g(\alpha)$ represents the glass transition temperature depending on the degree of curing, and can be expressed as follows [34,35]:

$$T_g(\alpha) = \mathrm{T_{g0}} + \left(\mathrm{T_{g\infty}} - \mathrm{T_{g0}}\right)\frac{\lambda\alpha}{1-(1-\lambda)\alpha}, \quad (9)$$

where $\mathrm{T_{g0}}$ is the glass transition temperature of the uncured ($\alpha = 0$) matrix, and $\mathrm{T_{g\infty}}$ represents the glass transition temperature of the fully cured ($\alpha = 1$) matrix; λ is the material parameter.

In order to describe changes in the Poisson's ratio during phase transitions, we considered that during phase transitions, the bulk compression modulus does not change as significantly as does the elastic modulus. For example, according to some studies [23,24] the bulk compression modulus exhibits a reduction of only 2.5 times during the transition to the rubber-like state. Therefore, we used the following expression for changes in the bulk compression modulus:

$$K_m(T^*) = \begin{cases} K_m^0, & T^* > \mathrm{T_{g\infty}} - 80\ ℃ \\ K_m^\infty + \frac{T^*}{\mathrm{T_{g\infty}} - 80℃}(K_m^0 - K_m^\infty), & \mathrm{T_{g\infty}} - 80\ ℃ \geq T^* > 0\ ℃, \\ K_m^\infty, & T^* \leq 0\ ℃ \end{cases} \quad (10)$$

where K_m^0, and K_m^∞ represents the bulk compression modulus of polymerized matrix at temperatures of 20 ℃, and $\mathrm{T_{g\infty}}$.

Then, we calculate the Poisson's ratio using the classical relation as follows:

$$\nu_m = \frac{3K_m - E_m}{6K_m}. \quad (11)$$

In this work, we describe the formation of cracks at the surface of the pultruded rod. The crack forms immediately after the die exit (see Figure 1a) and propagates along the profile (Figure 1b). Opening of the crack after initiation, as shown in Figure 1c, indicates the existence of transverse tension stresses in the crack formation region. As this takes place, the temperature at the surface of the profile exceeds the glass transition temperature of the material. Considering the symmetry of the profile cross section as well as the presumed position of the crack at the surface of the product, we assume that the strength of the composite can be deemed sufficient if transverse stresses (e.g., stresses σ_{xx} at the axis y (see Figure 2)) do not exceed the tensile strength of the matrix, i.e.,

$$\sigma_{xx}(0, y) < \sigma_u(T) = \begin{cases} \sigma_u^0, & T \leq 20\ ℃; \\ \sigma_u^0 + \frac{T - 20\ ℃}{20℃}(\sigma_u^1 - \sigma_u^0), & 40\ ℃ \geq T > 20\ ℃; \\ \sigma_u^1 + \frac{T - 40\ ℃}{20℃}(\sigma_u^2 - \sigma_u^1), & 60\ ℃ \geq T > 40\ ℃; \\ \sigma_u^2 + \frac{T - 60\ ℃}{20℃}(\sigma_u^3 - \sigma_u^2), & 80\ ℃ \geq T > 60\ ℃; \\ \sigma_u^3 + \frac{T - 80\ ℃}{\mathrm{T_{g\infty}} - 80\ ℃}(\sigma_u^\infty - \sigma_u^3), & \mathrm{T_{g\infty}} \geq T > 80\ ℃; \\ \sigma_u^\infty, & T > \mathrm{T_{g\infty}} \end{cases} \quad (12)$$

where σ_u^0, σ_u^1, σ_u^2, σ_u^3, and σ_u^∞ represent the strength of the polymerized matrix at temperatures of 20 ℃, 40 ℃, 60 ℃, 80 ℃, and $\mathrm{T_{g\infty}}$, respectively. Here, the values σ_u^0, σ_u^1, σ_u^2, and σ_u^3 are determined experimentally, and the value of σ_u^∞ is taken such that it correlates with experimental observations where cracks are formed at the pulling speed of 5 cm/min.

In order to describe the mechanical behavior of the composite, we used the self-consistent field micromechanics (SCFM) approach [36–38]. In order to calculate displacements and stresses, we used the incremental linear elastic approach [14] implemented in the ABAQUS environment [39]. The following user subroutines were used: UMAT, FILM, USDFLD, HETVAL, UEXPAN, and UEXTERNALDB. Computer files of user subroutines and ABAQUS computational models, together with a detailed description of mathematical relations, can be found at the GitHub repository [40]. The developed modeling method is also applicable for process optimization of thick composite products using other technologies [22,41–43].

Experimental Methods to Determine Model Parameters

The relationships between the elastic modulus and the temperature, which are determined using the dynamic mechanical analysis (DMA) method, may depend to a large degree on experiment conditions and loading type. Moreover, they may differ from data obtained by the mechanical tensile testing of resin samples [44]. Therefore, in this work, the elastic modulus and the tensile strength of cured resin at different temperatures (T = 20, 40, 60, and 80 °C) were determined experimentally in accordance with the ISO 527-2 standard [45] using the Instron 8801 (Instron, USA) testing machine equipped with a thermal camera. We tested five samples at each temperature, and the average values obtained are given in Table 1.

The glass transition temperature of a fully cured resin was measured using the DMA methods employing the DMA Q800 system (TA Instruments, USA). Three samples were tested at an oscillation frequency of 1 Hz and a heating rate of 5 °C/min; the average values of the glass transition temperature are given in Table 1.

In order to determine the polymerization kinetics parameters, we used a TA 3000 DSC 20 (Mettler Toledo, USA) differential scanning calorimeter in dynamic mode. The heating rate

constituted 10 °C/min, with a sample weight of 20 mg. Results of data processing for four experiments are given in Table 1.

The relation between the heat capacity of the composite material and the temperature and degree of polymerization was determined using the mixtures rule, and was based on the corresponding heat capacity data for a fully polymerized composite, neat resin (without accelerator), and E-glass. Temperature dependencies of the heat capacity for the materials studied were determined by performing differential scanning calorimetry (DSC) methods using a TA-990 (DuPont, USA) calorimeter at a heating rate of 10 °C/min. In order to describe the temperature dependencies obtained, we used linear relations with parameters determined by the least-squares method. The resulting expression for heat capacity dependence on temperature and degree of polymerization is given in Table 1.

Optimization

Here, we consider a single-criterion optimization problem involving the maximization of the pulling speed:

$$\text{Maximize pulling speed } u; \tag{13}$$

while satisfying the following constraints:

1) the thermal destruction of the material must be avoided: $\max_{\{x,y,z\}} T < T_d$, (14)

2) the temperature of the material by the end of the process must be lower than $T_{g\infty}$:

$\max_{\{x,y,L_{die}+L_{line}\}} T < T_{g\infty}$, (15)

3) the degree of polymerization at the end of the process should exceed 0.9

$\min_{\{x,y,L_{die}+L_{line}\}} \alpha > 0.9$, (16)

4) transverse stresses must not exceed the strength of the matrix (12) $\sigma_{xx_{max}}/\sigma_u < 1.0$. (17)

In order to solve the optimization problem, we used the surrogate-based optimization method implemented in the pSeven [46] software suite. The basis of this method is the global optimum search algorithm based on surrogate models, which are themselves based on Gaussian processes [47,48].

During optimization, the algorithm sequentially builds a series of surrogate models describing the desired function. A surrogate model is built based on design space exploration data [46]. The results of surrogate model construction are further used to build regions describing the constraints in the optimum search problem.

Results and discussions

This study was conducted to determine the causes of crack formation on the surface of the solid pultruded profile with a diameter of 80 mm, as observed by the increase in pulling speed. The profile is fabricated at the ApATeCh factory (the city of Dubna, Russia) using a Px-500-6T pultrusion machine (Pultrex, UK). The matrix used is a composition that is based on the epoxy diane resin with isomethyltetrahydrophthalic anhydride as a hardener and dimethyldodecylamine as an accelerator. The reinforcement is a 9600 tex glass fiber roving. The volume fraction of reinforcement is 65%. Crack formation was observed as the pulling speed increased to 5 cm/min. The die block has a length of 1 m, and has two heating zones with temperatures of $T_1 = 150$ °C in the first zone and $T_2 = 190$ °C in the second zone. The die block temperatures were measured with thermocouples installed at several points along the length of the die block; measurement results are given in Table 1.

The values of model parameters used in the computations are listed in Table 1. The table also includes information on the source of data. As the profile section is symmetric, only a quarter of the model is used in the analysis, and contains 363 linear quadrilateral elements of CPE4RT type (see Figure 1a). Symmetrical boundary conditions are set for AB and AC edges

(see Figure 1a). Within the die block region, at the outer perimeter (the BC segment in Figure 1a) of the profile, we set mechanical contact boundary conditions for interactions with the rigid surface, simulating the inner surface of the die block. After the die block exit, the contact boundary conditions are deactivated. Besides, at the outer perimeter of the profile, we set the boundary conditions of thermal contact with the ambient air, with the given coefficient of convective heat transfer. Very high values of the convective heat transfer coefficient are set for the profile located within the die block ($h_{die} = 5000.0$ W/(m2°C)) to simulate perfect thermal contact with the die block, the temperature of which is modeled by linear approximation based on experimentally measured values at the die block (see Table 1). After the die block exit, we simulate the thermal contact with the ambient air using a convective heat transfer coefficient of $h_{air} = 10.0$ W/(m2°C) and an ambient temperature of $T_{amb} = 25$ °C.

Table 1. Model parameters.

Property	Source	Symbol	Value	Unit
Heat conductivity problem				
Density of composite	[49]	ρ_c	2105	$^{kg}/_{m^3}$
Density of resin	[49]	ρ_r	1260	$^{kg}/_{m^3}$
Thermal conductivity of the composite in the transverse direction	[49]	k	0.5689	$^{W}/_{m\ ºC}$
Heat capacity of the composite depending on the temperature and degree of polymerization	–b	$C_{pc}(T,\alpha)$	976+0. 17·T-18·α+7.7·α·T	J/(kg·ºC)
The coefficient of convective heat transfer between the ambient air and the profile after the die block exit	[14]	h_{air}	10.0	W/(m^{2}ºC)
The coefficient of convective heat transfer between the die block and the profile	–e	h_{die}	5000.0	W/(m^{2}ºC)
Cure kinetics				
Pre-exponential coefficient	–b	A_0	4.3652·10^5	1/s
Activation energy	–b	E_a	66.4	kJ/mol
Order of reaction	–b	n	1.17	-
Total heat released	–b	H_R	373.0	kJ/kg
Temperature conditions				
Temperature at the die block, $T_{die}(z)$				
@ 0 cm (at the die block entrance)	–a	T_0	75	°C
@ 30–50 cm (1st heating zone)	–a	T_1	150	°C
@ 60–80 cm (2nd heating zone)	–a	T_2	190	°C
@ 100 cm (at the die block exit)	–a	T_3	160	°C
Temperature of material at the die block entrance	–a	T_{in}	50	°C
Ambient temperature	–a	T_{amb}	25	°C
Mechanical properties of the polymer				
Young's modulus at $T = 20\ °C$	–c	E_m^0	3475	MPa
Young's modulus at $T = 40\ °C$	–c	E_m^1	3277	MPa
Young's modulus at $T = 60\ °C$	–c	E_m^2	3025	MPa
Young's modulus at $T = 80\ °C$	–c	E_m^3	2321	MPa
Young's modulus at $T = \mathrm{T_{g\infty}}$	$\frac{9K_m^\infty G_m^\infty}{3K_m^\infty + G_m^\infty}$	E_m^∞	37.69	MPa
Tensile strength at $T = 20\ °C$	–c	σ_u^0	51.1	MPa
Tensile strength at $T = 40\ °C$	–c	σ_u^1	44.9	MPa

Tensile strength at $T = 60\ °C$	–c	σ_u^2	38.8	MPa
Tensile strength at $T = 80\ °C$	–c	σ_u^3	30.0	MPa
Tensile strength at $T = \mathrm{T_{g\infty}}$	–e	σ_u^∞	1.03	MPa
Poisson's ratio at $T = 20\ °C$	[24]	ν_m^0	0.38	-
Shear modulus at $T = 20\ °C$	$\frac{E_m^0}{2(1+\nu_m^0)}$	G_m^0	1259	MPa
Shear modulus at $T = \mathrm{T_{g\infty}}$	$G_m^0/100$ [24]	G_m^∞	12.59	MPa
Bulk modulus at $T = 20\ °C$	$\frac{E_m^0}{3(1-2\nu_m^0)}$	K_m^0	4826	MPa
Bulk modulus at $T = \mathrm{T_{g\infty}}$	$K_m^0/2.5$ [24]	K_m^∞	1931	MPa
Coefficient of thermal expansion at $T = 20\ °C$	[36]	α_m^0	$5.76{\cdot}10^{-5}$	1/°C
Coefficient of thermal expansion at $T = \mathrm{T_{g\infty}}$	$2.5\alpha_m^0$ [36]	α_m^∞	$14.4{\cdot}10^{-5}$	1/°C
Mechanical properties of glass fiber reinforcement				
Young's modulus	[36]	E_f	73 080	MPa
Poisson's ratio	[36]	ν_f	0.22	
Coefficient of thermal expansion	[36]	α_f	$5.04{\cdot}10^{-6}$	1/°C
Other properties				
Pulling speed	–a	u	5.0	cm/min
The volume fraction of reinforcement	–a	V_f	0.65	-
Total volumetric chemical shrinkage	[24]	ΔV	-7	%
$\mathrm{T_g}$ at $\alpha = 0$	[24]	$\mathrm{T_{g0}}$	-41	°C
$\mathrm{T_g}$ at $\alpha = 1$	–d	$\mathrm{T_{g\infty}}$	101.5	°C
Material constant in (5)	[24]	λ	0.44	-
Die block length	–a	L_{die}	1.0	m
The length of pultrusion machine section between the die block exit and a cut-off saw	–a	L_{line}	5.0	m
Thermal destruction temperature of resin	[50]	T_d	240	°C

a. Measured value

b. Determined from DSC data.

c. Determined from mechanical testing.

d. Determined from DMA data.

e. Assumed value.

Figure 2 shows simulation results that were obtained for the given case. Figure 2b-d shows results obtained for the section located immediately after the die exit. The thickness of the polymerized layer of material (degree of polymerization exceeds 0.9) constitutes approximately 10 mm (see Figure 2c). The temperature of the material in the polymerized region ranges from 160 to 170 °C. The temperature of the material at the core of the profile is 100 °C (see Figure 2b). Transverse stresses are positive in the region of the polymerized material, with a maximum stress of 1.02 MPa (see Figure 2d). Figure 2e-g shows the changes in temperature (Figure 2e), degree of polymerization (Figure 2f), and transverse stress (Figure 2g) along the length of the die block, measured at different points on a vertical axis, with the following coordinates $y = 0.0$ mm (center), $y = 0.016$ mm, $y = 0.029$ mm, $y = 0.04$ mm (surface of the profile) (see Figure 2a). An exothermic peak can be observed at 20 cm after the die block exit at the core of the profile ($y = 0.0$ mm), with a maximum temperature reaching 201 °C (see Figure 2e). At the same distance from the die block, the degree of material polymerization exceeds 0.9 over the entire cross section (see Figure 2f). It should be noted that at the segment located between the exothermic peak position and up to 2.5 m after the die exit, the temperature of the material exceeds the glass transition temperature, $T_{g\infty}$, over the entire cross section of the profile. Only at the distance of 4.2 m after the die block exit does the material temperature decrease below $T_{g\infty}$ (see Figure 2e). Transverse stresses are positive at the surface layer ($y = 0.029$ mm, $y = 0.04$ mm), where the degree of polymerization exceeds 0.9 immediately after the die exit, and they start to decrease as the profile is pulled further, reaching negative values by the end of the process (see Figure 2g). At the same time, transverse stresses at the center of the profile are negative, and they increase as the profile is pulled further, reaching positive values (0.8 MPa) by the end of the process. If we extrapolate to the moment at which the temperature difference over

the entire cross section does not exceed 0.1 °C (i.e., when the profile is cooled to the ambient temperature T_{amb}=25 °C), the stress at the surface of the profile will be approximately $\sigma_{xx}(0,0.04,\infty) = -7.8$ MPa, and near the center of the profile, $\sigma_{xx}(0,0,\infty) = 2.7$ MPa. The order of magnitude of the obtained stress values is in good agreement with the experimental values of the residual stress for the unidirectionally reinforced pultrusion profile obtained using the digital image correlation method in combination with the hole drilling technique (see [51]). The experimental value of the residual transverse stress at the core of the profile, as reported in [51], has a tension of 6.1 MPa, which is higher compared to the value of 2.7 MPa obtained in this work. This can be attributed to the lower chemical shrinkage of epoxy resin that we used in this study compared to the polyester resin used in [51]. Besides, the volume fraction of resin in [51] is also higher relative to the value used in this study. In addition, it should be noted that the obtained stresses are an order of magnitude less than the strength of the matrix under normal conditions (see Table 1).

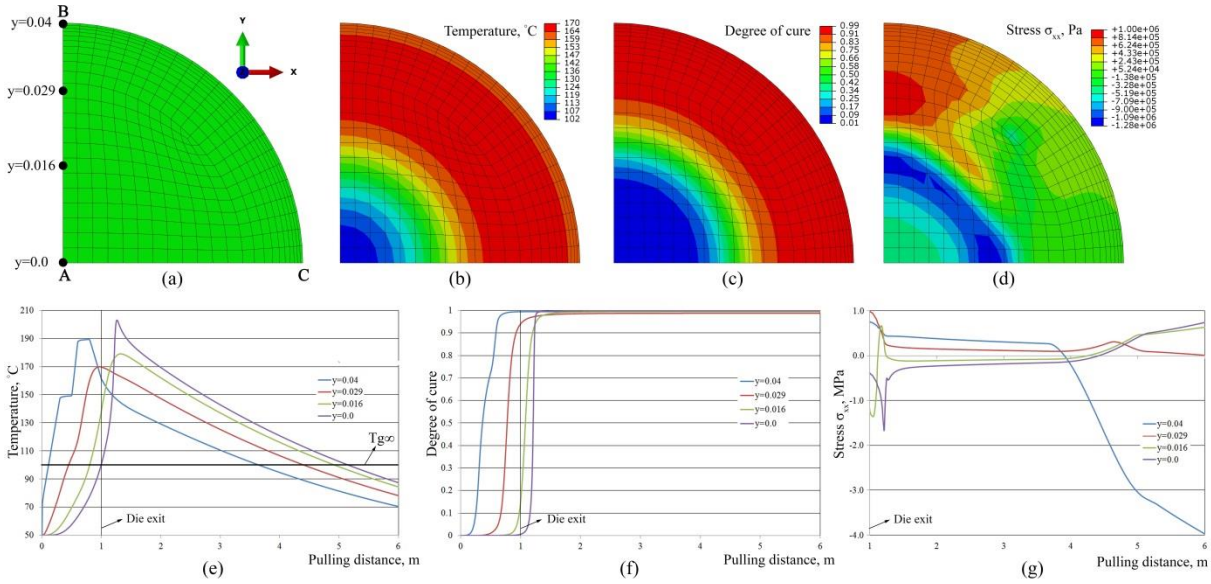

Figure 2. Simulation results for the 80 mm diameter rod at the pulling speed of $u = 5$ cm/min when the crack is formed after the die exit (only a quarter of the model is shown): (a) – finite-element mesh used in the study; (b)–(d) simulation results at the cross section after the die exit (b) – temperature; (c) – degree of polymerization; (d) – stress σ_{xx}; (e)–(g) graphs of temperature (e), degree of polymerization (f), and stress, σ_{xx}; (g) changes along the length of a die block measured at different points on a vertical axis with the following coordinates $y = 0.0$ mm (center), $y = 0.016$ mm, $y = 0.029$ mm, and $y = 0.04$ mm (surface of the profile).

Figure 3 shows simulation results obtained for the maximum transverse stress for different pulling speeds as well as for different values of chemical shrinkage, ΔV, assuming that the temperature of the material exceeds $T_{g\infty}$. Figure 3a shows simulation results obtained for the proposed models of elastic modulus (8) and Poisson's ratio (11); in Figure 3b, the Poisson's ratio of the matrix is assumed constant, $\nu_m = 0.38$. We can see that an increase in the pulling speed results in an increased maximum transverse stress (see Figure 3a), which is in good agreement with the experimental data showing that an increase in the pulling speed results in the formation of cracks. Considering that cracks open as the profile is pulled further, they can be attributed to the increase in positive transverse tensile stress. The lower volumetric chemical shrinkage ΔV results in lower maximum transverse stresses. For the case considered here, a reduction in chemical shrinkage, ΔV, from -7% to -3% results in a 56% decrease in the transverse stress to 0.45 MPa at a pulling speed of 5.0 cm/min (see Figure 3a). Thus, the value

of volumetric chemical shrinkage ΔV has a significant influence on the maximum transverse stress, and thus the potential for crack formation. From this research, it is evident that the application of anti-shrink additives can make it possible to increase pulling speeds owing to the reduced maximum transverse stress causing the formation of cracks. Assuming a constant Poisson's ratio, we can observe a similar increase in the maximum transverse stress with increased pulling speed. However, the stress values are significantly lower, e.g., for the case considered; at the pulling speed of 5 cm/min, the decrease in the maximum transverse stress was 46%, for the value of 0.55 MPa (see Figure 3b).

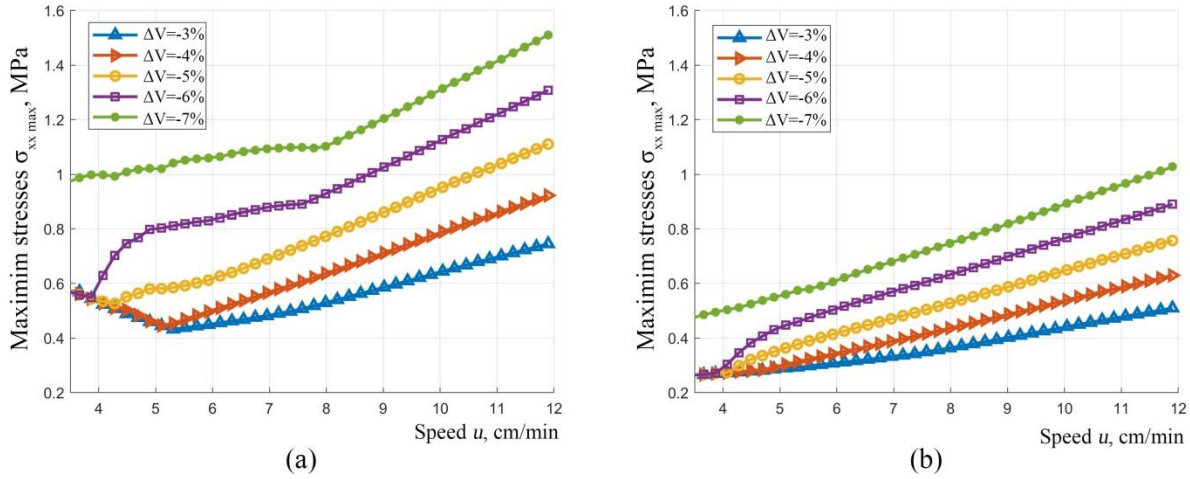

Figure 3. Maximum transverse stresses as a function of pulling speed for different values of chemical shrinkage, ΔV, assuming that the temperature of the material exceeds $T_{g\infty}$. (a) matrix elastic modulus is determined from (8) and Poisson coefficient is determined from (11); (b) matrix elastic modulus is determined from (8), and the Poisson coefficient is assumed constant $\nu_m = 0.38$.

Table 2 shows results of the temperature condition optimization required to maximize the pulling speed (13). The following temperature variation ranges were considered: temperature of the material at the die entrance, T_{in}, from 20 to 70 °C; temperature at the 1st heating zone, T_1, from 120 to 170 °C; and temperature at the 2nd heating zone, T_2, from 150 to 200 °C. The results show that the pulling speed can be increased by 27% from an initial speed of

5.00 cm/min (initial scenario, see Table 2) to 6.36 cm/min, provided that the quality criteria (14)–(17) are met (optimum scenario, see Table 2).

Table 2. Results of temperature condition optimization.

	Parameters				Constraints			
	u, cm/min	T_{in}, °C	T_1, °C	T_2, °C	T_{end}, °C (14)	T_{max}, °C (15)	α_{min} (16)	$\sigma_{xx_{max}}/\sigma_u$ (17)
Boundaries	-	20–70	120–170	150–200	<101.5	<240.0	>0.90	<1.0
Initial	5.00	50	150	190	99.7	202.9	0.99	0.99
Optimum	6.36	55	170	170	101.4	194.6	0.96	0.99

To construct regions representing the compliance or violation of constraints, we built four surrogate models (for the degree of polymerization, stress, maximum temperature, and maximum temperature in the last section). Based on 168 design points, the precision of the surrogate model construction was assessed using the root mean square error (RMSE), and was:

1) 0.013 for the degree of curing model;
2) 0.0203 for the maximum transverse stress model;
3) 0.1449 for the maximum temperature model;
4) 0.1843 for the model of the maximum temperature in the last section.

Figure 4 shows regions representing the compliance with quality criteria for varying pulling speeds u and material temperatures at the die entrance, T_{in}. Diagrams shown in Figure 4 are based on the data of approximation model application. Figure 4a shows the initial scenario when the temperature at the 1st zone of the die block is equal to T_1= 150 °C, and the temperature at the 2nd zone is equal to T_2= 190 °C (see Table 1). Figure 4b shows the optimum scenario with T_1= 170 °C, and T_2= 170 °C, (see Table 2). At low pulling speeds (u< 4.3 cm/min), all criteria are satisfied for all temperatures of material at the die entrance

(yellow region) 20 °C $\leq T_{in} \leq$ 70 °C). With the increase in the pulling speed, the criterion of the material strength is violated, i.e., the transverse stress exceeds the strength of the material (blue region). At the same time, the allowable pulling speed for the optimum scenario can be increased (see Figure 4b) by increasing the T_{in} temperature to 55 °C. A further increase in the temperature T_{in} results in the profile having insufficient time to cool down below the glass transition temperature, $T_{g\infty}$ (green zone). Therefore, the obtained optimum point acts as a boundary point for two criteria simultaneously, accounting for crack formation and profile overheating at the end of the process (see Table 2, Figure 4b). A further increase in the pulling speed will also result in a lower degree of polymerization by the end of the process (blue region).

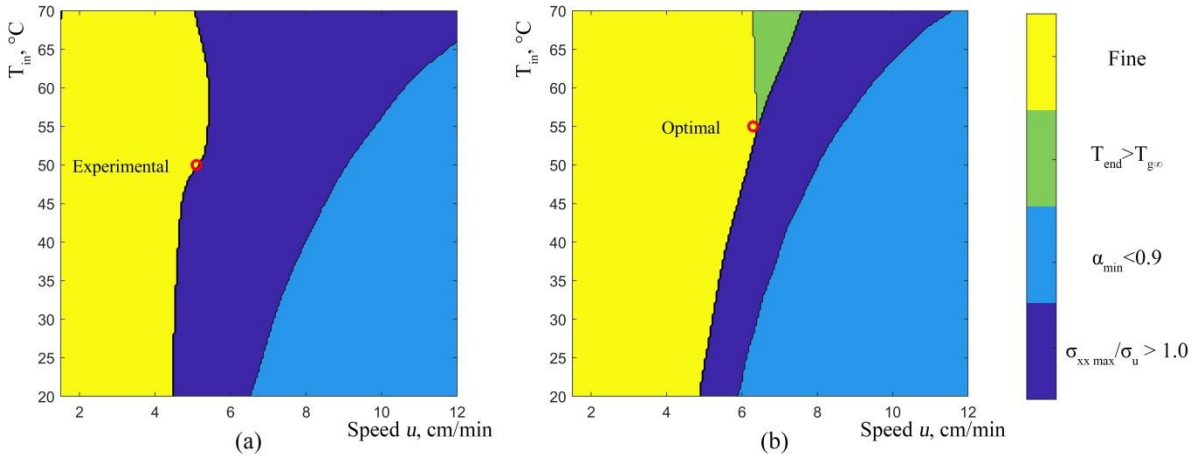

Figure 4. Regions representing compliance with quality criteria for varying pulling speeds, u, and material temperatures at the die entrance, T_{in}: (a) initial scenario with T_1= 150°C and T_2= 190°C; (b) optimum scenario with T_1= 170°C and T_2= 170°C.

In [20], a simulation of the pultrusion process of a 100 × 100 mm square section glass/polyester profile is discussed; this was conducted to understand the formation of cracks inside a pultruded profile during fabrication. Cracks are formed at diagonals through opposite vertices of a square section, and are located at a certain distance from the surface of the

profile. In [20], these cracks are attributed to the high level of transverse shear stresses observed in these areas by the end of the process. However, we believe that in terms of their formation mechanism, these cracks are similar to the cracks at the surface of the 80-mm pultruded rod considered here. In order to prove our assumptions, we conducted simulations for a 100 × 100 mm square section profile. A quarter of a model was considered with the same model parameters as in the case of the 80 mm diameter rod (see Table 1). Figure 5 shows simulation results for the cross section of a 100 mm × 100 mm square section profile immediately after the die exit. The thickness of the polymerized layer of material (degree of polymerization exceeds 0.9) in the narrowest part of the layer is approximately 8 mm (see Figure 5b). The temperature of the material at the core of the profile is 64 °C (see Figure 5b). The region with the maximum values of the maximum in-plane principal stress σ_1 is located at the diagonal at a distance of 20 mm from the surface of the profile (see Figure 5c). Maximum value σ_1 is approximately 2.0 MPa. The principal axes of stress σ_1 in this area are oriented tangentially to the polymerization front (see Figure 5c). The region with the maximum values of the minimum in-plane principal stress σ_2 is also located in this area (see Figure 5d). The maximum value of σ_2 is approximately 1.1 MPa. The principal axes of stress σ_2 in this area are oriented perpendicular to the polymerization front (see Figure 5d). In accordance with the strength criterion accepted in this work (12), this area will undergo crack formation under the influence of both σ_1 stress and σ_2 stress. Therefore, the proposed model can also explain the formation of cracks in a square section profile with an area of 100 × 100 mm, which can be observed experimentally.

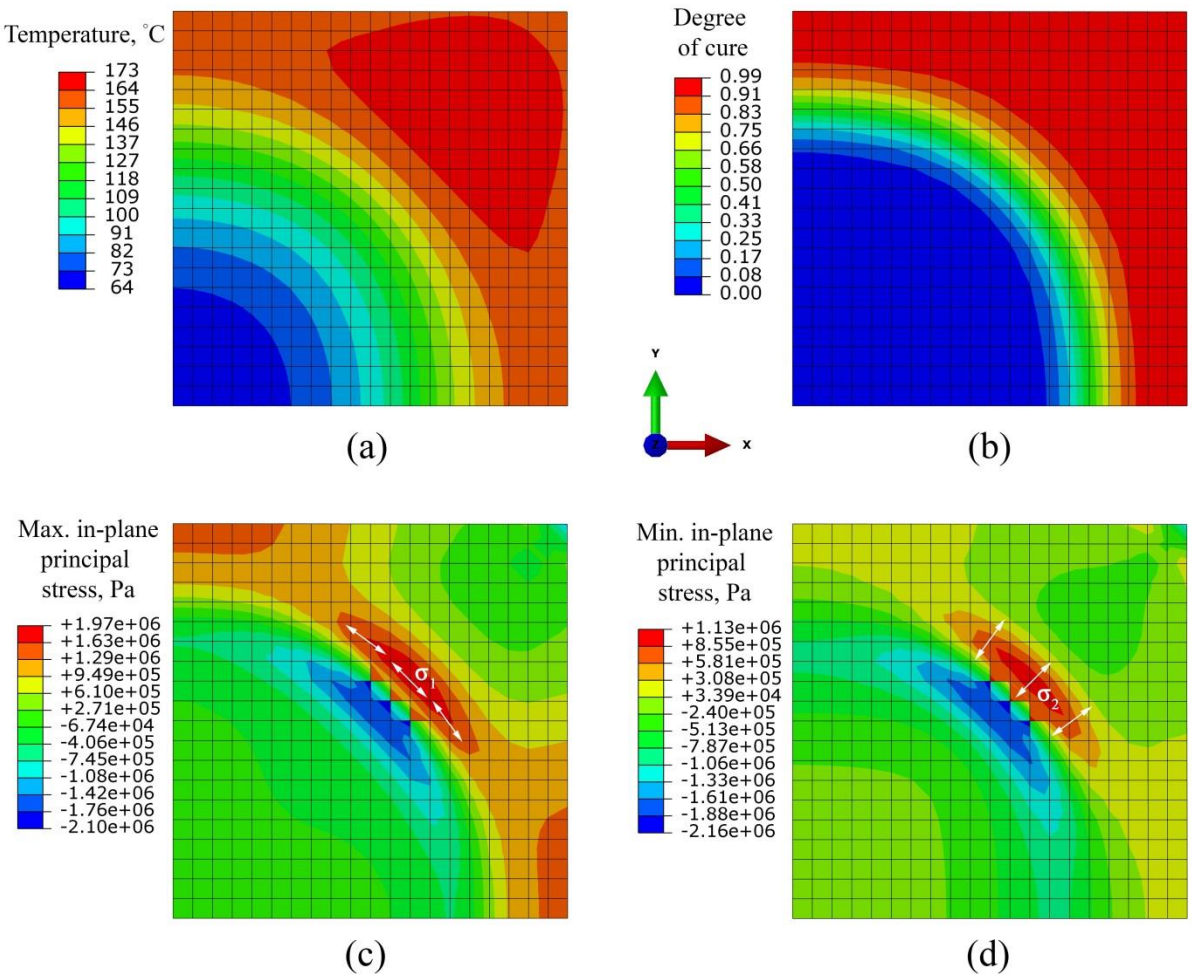

Figure 5. Simulation results for the square section profile of 100 mm × 100 mm in a section immediately after the die exit (a quarter of the model is considered): (a) temperature; (b) degree of polymerization; (c) maximum in-plane principal stress, σ_1; and (d) minimum principal stress, σ_2.

In this paper, a model for crack formation in a pultruded composite profile is proposed. The model describes the formation of cracks in a material immediately after polymerization, caused by significant non-uniformity in the distribution of temperatures and the degree of polymerization existing in a product. Such "cure-induced" cracks differ in their size and location from matrix cracking [27], which occurs as a result of residual stresses acting on the material during cooling. For example, for the 80 mm diameter rod studied here, cure-induced cracks form at the surface of the product. However, based on simulations of residual stresses, matrix cracking should take place at the core of the profile, where positive transverse stresses

exist at the end of the process (see Figure 2g). Moreover, we were able to observe experimentally the formation of cure-induced cracks together with matrix cracking during the pultrusion of the L-shaped profile (75 mm × 75 mm, with a wall thickness of 6 mm). We used a Px500-6T pultrusion machine at the Laboratory of Composite Materials and Structures of The Center for Design, Manufacturing, and Materials (Skolkovo Institute of Science and Technology, Moscow, Russia). Matrix cracks go through the whole thickness of the internal layer of the unidirectional material. However, cure-induced cracks are located along the centerline of the profile cross section, i.e., they are located perpendicular to matrix cracks. The thickness of cure-induced cracks is approximately 1 mm, which is significantly higher compared to the thickness of matrix cracks (0.2 mm). Owing to the position of the cure-induced cracks and their large thickness, these cracks may result in significant geometrical distortions. The influence of the pulling speed on cure-induced and matrix cracking, as well as on shape distortions during the pultrusion of L-shaped profiles will be discussed in detail in future works. Modeling of technological defects formation and their influence on mechanical properties for other standard types of profiles [52] and new types designed using topological optimization methods [53] will also be carried out.

For the case of the pultruded 80 mm diameter rod considered here, only a 10 mm thick surface layer is fully polymerized inside the die block. Then, after exiting the die block, the polymerization front shifts to the center of the profile because of the heat released during polymerization. This mechanism of polymerization in thick pultruded profiles is an example of frontal polymerization during pultrusion. Thus, the authors believe that the proposed numerical simulation method can be applied to understand the formation of potential defects during the implementation of frontal polymerization [54].

Conclusion

A numerical simulation of the pultrusion process of 80 mm diameter glass/epoxy rod was conducted to understand the phenomenon of crack formation at the surface of a profile after the die exit at increased pulling speeds. Resin polymerization kinetics and the temperature dependence of the heat capacity were determined using DSC methods. The glass transition temperature of resin was determined by performing DMA methods. Changes in the elastic modulus and strength of polymerized resin were determined experimentally by mechanical tensile testing according to the ISO-527-2 standard. We used a modified CHILE model, accounting for changes in the elastic modulus and Poisson coefficients during phase transitions.

. In order to accelerate the computations, a 2D setting was considered both for the problem of thermal conductivity and the degree of polymerization distribution, as well as for the problem of stress-strain state calculation. The SCFM approach was used to describe the mechanical behavior of a composite. The developed model was implemented in ABAQUS environment; computer files of user subroutines and ABAQUS computational models, together with a detailed description of the mathematical relations, can be found at the GitHub repository.

Using the proposed resin strength criterion, which is dependent on the material temperature, we modeled crack formation at the surface of the rod immediately after the die exit, as the polymerized layer contains positive transverse stress and the material temperature exceeds the glass transition temperature. Positive transverse stresses in a polymerized layer after the die exit were found to increase as the pulling speed increased, which is in good agreement with the experimental data. We also determined the criteria for the analysis of temperature as well as the degree of polymerization and residual stress fields, which are intended to ensure the quality of manufactured profiles. The optimization of temperature conditions was conducted using the pSeven software suite to enable an increase in pulling speed considering the

proposed quality criteria. The results show that the pulling speed can be increased by 27% from an initial speed of 5.00 cm/min (initial scenario, see Table 2) to 6.36 cm/min (optimum scenario, see Table 2), provided that the quality criteria (14)–(17) are met. In addition, the successful simulation of the pultrusion process of a 100 mm × 100 mm square section glass/polyester profile was conducted to explain the formation of cracks inside a pultruded profile, which was observed experimentally during fabrication.

Acknowledgement

The authors would like to thank the employees of the company ApATeCh, Tatyana Sorina and Alexander Khayretdinov, for providing the experimental data and for the discussion of simulation results. This research did not receive funding from any funding agencies in the public, commercial, or not-for-profit sectors.

References

[1] Starr TF. Pultrusion for engineers. 2000. doi:10.1533/9781855738881.97.

[2] Fairuz AM, Sapuan SM, Zainudin ES, Jaafar CNA. Polymer composite manufacturing using a pultrusion process: A review. Am J Appl Sci 2014;11. doi:10.3844/ajassp.2014.1798.1810.

[3] Sumerak JE. Pultrusion Process Troubleshooting. Handb. Troubl. Plast. Process. A Pract. Guid., 2012. doi:10.1002/9781118511183.ch20.

[4] Creative Pultrusions. The Pultex® Pultrusion Design Manual. 2017.

[5] Fibreforce. Design Manual – Engineered Composite Profiles. n.d.

[6] Baran I. Pultrusion: state-of-the-art process models. Shropshire: Smithers Rapra; 2015.

[7] Safonov AA, Carlone P, Akhatov I. Mathematical simulation of pultrusion processes: A review. Compos Struct 2018;184. doi:10.1016/j.compstruct.2017.09.093.

[8] Suratno BR, Ye L, Mai Y-W. Simulation of temperature and curing profiles in pultruded composite rods. Compos Sci Technol 1998;58:191–7. doi:10.1016/S0266-3538(97)00132-2.

[9] Voorakaranam S, Joseph B, Kardos JL. Modeling and control of an injection pultrusion process. J Compos Mater 1999;33:1173–204. doi:10.1177/002199839903301302.

[10] Liu X-L. A finite element/nodal volume technique for flow simulation of injection pultrusion. Compos Part A Appl Sci Manuf 2003;34:649–61. doi:10.1016/S1359-835X(03)00085-X.

[11] Safonov a. a. Mathematical description of the technological process of injection pultrusion. J Mach Manuf Reliab 2011;40:68–73. doi:10.3103/S1052618811010171.

[12] Raper KS, Roux JA, McCarty TA, Vaughan JG. Investigation of the pressure behavior in a pultrusion die for graphite/epoxy composites. Compos Part A Appl Sci Manuf 1999;30:1123–32. doi:10.1016/S1359-835X(98)00196-1.

[13] Carlone P, Baran I, Hattel JH, Palazzo GS. Computational approaches for modeling the multiphysics in pultrusion process. Adv Mech Eng 2013;2013. doi:10.1155/2013/301875.

[14] Baran I, Tutum CC, Nielsen MW, Hattel JH. Process induced residual stresses and distortions in pultrusion. Compos Part B Eng 2013. doi:10.1016/j.compositesb.2013.03.031.

[15] Baran I, Akkerman R, Hattel JH. Modelling the pultrusion process of an industrial L-shaped composite profile. Compos Struct 2014;118:37–48. doi:10.1016/j.compstruct.2014.07.018.

[16] Carlone P, Palazzo GS, Pasquino R. Pultrusion manufacturing process development: Cure optimization by hybrid computational methods. Comput Math with Appl 2007;53:1464–71. doi:10.1016/j.camwa.2006.02.031.

[17] Baran I, Tutum CC, Hattel JH. Optimization of the thermosetting pultrusion process by using hybrid and mixed integer genetic algorithms. Appl Compos Mater 2013;20:449–63. doi:10.1007/s10443-012-9278-3.

[18] Safonov AA, Suvorova YV. Optimization of the pultrusion process for a rod with a large diameter. J Mach Manuf Reliab 2009;38. doi:10.3103/S1052618809060090.

[19] Safonov AA, Saratov AA, Ushakov AE. Numerical optimization and sensitivity analysis of pultrusion process parameters. ECCM 2016 - Proceeding 17th Eur. Conf. Compos. Mater., 2016.

[20] Baran I. Analysis of pultrusion process for thick glass/polyester composites: transverse shear stress formations. Adv Manuf Polym Compos Sci 2016;2:124–32. doi:10.1080/20550340.2016.1269037.

[21] Sorrentino L, Tersigni L. A method for cure process design of thick composite components manufactured by closed die technology. Appl Compos Mater 2012;19:31–

45. doi:10.1007/s10443-010-9179-2.

[22] Sorrentino L, Esposito L, Bellini C. A new methodology to evaluate the influence of curing overheating on the mechanical properties of thick FRP laminates. Compos Part B Eng 2017;109:187–96. doi:10.1016/j.compositesb.2016.10.064.

[23] Lindrose AM. Ultrasonic wave and moduli changes in a curing epoxy resin. Exp Mech 1978;18:227–32. doi:10.1007/BF02328418.

[24] Svanberg JM, Holmberg JA. Prediction of shape distortions Part I. FE-implementation of a path dependent constitutive model. Compos Part A Appl Sci Manuf 2004. doi:10.1016/j.compositesa.2004.02.005.

[25] Péron M, Sobotka V, Boyard N, Le Corre S. Bulk modulus evolution of thermoset resins during crosslinking: Is a direct and accurate measurement possible? J Compos Mater 2017. doi:10.1177/0021998316647119.

[26] Baran I, Hattel JH, Tutum CC, Akkerman R. Pultrusion of a vertical axis wind turbine blade part-II: combining the manufacturing process simulation with a subsequent loading scenario. Int J Mater Form 2015;8:367–78. doi:10.1007/s12289-014-1178-7.

[27] Drach B, Tsukrov I, Trofimov A, Gross T, Drach A. Comparison of stress-based failure criteria for prediction of curing induced damage in 3D woven composites. Compos Struct 2018;189:366–77. doi:10.1016/j.compstruct.2018.01.057.

[28] Baran I, Tutum CC, Hattel JH. Reliability estimation of the pultrusion process using the first-order reliability method (FORM). Appl Compos Mater 2013;20:639–53. doi:10.1007/s10443-012-9293-4.

[29] Costa Dias R de C, Santos L de S, Ouzia H, Schledjewski R. Improving degree of cure in pultrusion process by optimizing die-temperature. Mater Today Commun 2018. doi:10.1016/j.mtcomm.2018.08.017.

[30] Tutum CC, Baran I, Deb K. Optimum design of pultrusion process via evolutionary

multi-objective optimization. Int J Adv Manuf Technol 2014. doi:10.1007/s00170-014-5726-6.

[31] Batch GL, Macosko CW. Heat transfer and cure in pultrusion: Model and experimental verification. AIChE J 1993;39:1228–41. doi:10.1002/aic.690390713.

[32] Baran I, Hattel JH, Akkerman R, Tutum CC. Mechanical Modelling of Pultrusion Process: 2D and 3D Numerical Approaches. Appl Compos Mater 2014;22:99–118. doi:10.1007/s10443-014-9394-3.

[33] Johnston A. An integrated model of the development of process-induced deformation in autoclave processing of composite structures. University of British Columbia, 1997. doi:10.14288/1.0088805.

[34] Khoun L, Centea T, Hubert P. Characterization methodology of thermoset resins for the processing of composite materials -Case study. J Compos Mater 2010;44:1397–415. doi:10.1177/0021998309353960.

[35] O'Brien DJ, White SR. Cure Kinetics, Gelation, and Glass Transition of a Bisphenol F Epoxide. Polym Eng Sci 2003;43:863–74. doi:10.1002/pen.10071.

[36] Bogetti TA, Gillespie JW. Process-Induced Stress and Deformation in Thick-Section Thermoset Composite Laminates. J Compos Mater 1992;26:626–60. doi:10.1177/002199839202600502.

[37] White SR, Kim Y. Process-induced residual stress analysis of AS4/3501-6 composite material. Mech Compos Mater Struct 1998;5:153–86.

[38] Hill R. A self-consistent mechanics of composite materials. J Mech Phys Solids 1965;13:213–22. doi:10.1016/0022-5096(65)90010-4.

[39] Abaqus Analysis User Manual, Version 6.14. (2014). n.d. http://www.3ds.com/productsservices/.

[40] Safonov A, Konstantinov A. Abaqus user subroutines for numerical simulation of

cracking during pultrusion of 80 mm diameter GFRP rod 2019. https://github.com/AlexASafonov/Pultrusion.

[41] Bellini C, Sorrentino L. Analysis of cure induced deformation of CFRP U-shaped laminates. Compos Struct 2018;197:1–9. doi:10.1016/j.compstruct.2018.05.038.

[42] Esposito L, Sorrentino L, Penta F, Bellini C. Effect of curing overheating on interlaminar shear strength and its modelling in thick FRP laminates. Int J Adv Manuf Technol 2016;87:2213–20. doi:10.1007/s00170-016-8613-5.

[43] Sorrentino L, Polini W, Bellini C. To design the cure process of thick composite parts: Experimental and numerical results. Adv Compos Mater 2014;23:225–38. doi:10.1080/09243046.2013.847780.

[44] Deng S, Hou M, Ye L. Temperature-dependent elastic moduli of epoxies measured by DMA and their correlations to mechanical testing data. Polym Test 2007;26:803–13. doi:10.1016/j.polymertesting.2007.05.003.

[45] ISO-527-2. Plastics—determination of tensile properties—part 2: test conditions for moulding and extrusion plastics. Br Stand Inst 1997.

[46] DATADVANCE. pSeven. Available at: WwwDatadvanceCom/Product/Pseven 2016.

[47] Wang C, Duan Q, Gong W, Ye A, Di Z, Miao C. An evaluation of adaptive surrogate modeling based optimization with two benchmark problems. Environ Model Softw 2014. doi:10.1016/j.envsoft.2014.05.026.

[48] Koziel S, Leifsson L, Yang XS. Surrogate-based optimization. Simulation-Driven Des. Optim. Model. Microw. Eng., 2013. doi:10.1142/9781848169173_0003.

[49] Chachad YR, Roux JA, Vaughan JG, Arafat E. Three-Dimensional Characterization of Pultruded Fiberglass-Epoxy Composite Materials. J Reinf Plast Compos 1995;14:495–512. doi:10.1177/073168449501400506.

[50] Joshi SC, Lam YC, Win Tun U. Improved cure optimization in pultrusion with pre-

heating and die-cooler temperature. Compos Part A Appl Sci Manuf 2003;34:1151–9. doi:10.1016/j.compositesa.2003.08.003.

[51] Yuksel O, Baran I, Ersoy N, Akkerman R. Investigation of transverse residual stresses in a thick pultruded composite using digital image correlation with hole drilling. Compos Struct 2019;223. doi:10.1016/j.compstruct.2019.110954.

[52] Ascione F, Lamberti M, Razaqpur G. Modifications of standard GFRP sections shape and proportions for improved stiffness and lateral-torsional stability. Compos Struct 2015;132. doi:10.1016/j.compstruct.2015.05.005.

[53] Safonov AA. 3D topology optimization of continuous fiber-reinforced structures via natural evolution method. Compos Struct 2019;215:289–97. doi:10.1016/j.compstruct.2019.02.063.

[54] Robertson ID, Yourdkhani M, Centellas PJ, Aw JE, Ivanoff DG, Goli E, et al. Rapid energy-efficient manufacturing of polymers and composites via frontal polymerization. Nature 2018;557:223–7. doi:10.1038/s41586-018-0054-x.